

## Highlights

### **Spatiotemporal Heterogeneity of AI-Driven Traffic Flow Patterns and Land Use Interaction: A GeoAI-Based Analysis of Multimodal Urban Mobility**

Olaf Yunus Laitinen Imanov

- A GeoAI Hybrid framework combining MGWR, Random Forest, and Graph Neural Networks achieves  $RMSE = 0.119$  and  $R^2 = 0.891$  across three urban mobility modes, outperforming all benchmark models.
- SHAP analysis identifies land use mix as the dominant predictor for motor vehicle and active-mode flows, and transit stop density as the leading predictor for public transit.
- DBSCAN clustering yields five interpretable urban traffic typologies; Moran's  $I$  in model residuals falls from 0.782 (OLS) to 0.218 (GeoAI Hybrid), a 72% reduction.
- Within-morphology cross-city transfer achieves  $R^2 \geq 0.78$ ; cross-morphology transfer declines substantially, establishing practical limits for context-free GeoAI deployment.
- The framework provides planners with a spatially adaptive, interpretable toolkit for evidence-based land use and multimodal mobility policy design.

# Spatiotemporal Heterogeneity of AI-Driven Traffic Flow Patterns and Land Use Interaction: A GeoAI-Based Analysis of Multimodal Urban Mobility

Olaf Yunus Laitinen Imanov<sup>a,\*</sup>

<sup>a</sup>Department of Applied Mathematics and Computer Science (DTU Compute), Technical University of Denmark, Kongens Lyngby, Denmark

## ARTICLE INFO

### Keywords:

GeoAI  
spatiotemporal heterogeneity  
multimodal urban mobility  
geographically weighted regression  
land use mix  
graph neural networks  
traffic flow prediction  
urban spatial analytics

## ABSTRACT

Urban traffic flow is governed by the complex, nonlinear interaction between land use configuration and spatiotemporally heterogeneous mobility demand. Conventional global regression and time-series models cannot simultaneously capture these multi-scale dynamics across multiple travel modes. This study proposes a GeoAI Hybrid analytical framework that sequentially integrates Multiscale Geographically Weighted Regression (MGWR), Random Forest (RF), and Spatio-Temporal Graph Convolutional Networks (ST-GCN) to model the spatiotemporal heterogeneity of traffic flow patterns and their interaction with land use across three mobility modes: motor vehicle, public transit, and active transport. Applying the framework to an empirically calibrated dataset of 350 traffic analysis zones across six cities spanning two contrasting urban morphologies, four key findings emerge: (i) the GeoAI Hybrid achieves a root mean squared error (RMSE) of 0.119 and an  $R^2$  of 0.891, outperforming all benchmarks by 23–62 %; (ii) SHAP analysis identifies land use mix as the strongest predictor for motor vehicle flows ( $|\phi| = 0.184$ ) and transit stop density as the strongest predictor for public transit; (iii) DBSCAN clustering identifies five functionally distinct urban traffic typologies with a silhouette score of 0.71, and GeoAI Hybrid residuals exhibit Moran's  $I = 0.218$  ( $p < 0.001$ ), a 72 % reduction relative to OLS baselines; and (iv) cross-city transfer experiments reveal moderate within-cluster transferability ( $R^2 \geq 0.78$ ) and limited cross-cluster generalisability, underscoring the primacy of urban morphological context. The framework offers planners and transportation engineers an interpretable, scalable toolkit for evidence-based multimodal mobility management and land use policy design.

## 1. Introduction

Urban transportation networks are undergoing rapid transformation driven by accelerating urbanisation, the proliferation of data-generating infrastructure, and pressing policy demands around sustainability and modal equity [1, 2]. Traffic flow in contemporary cities is no longer a simple function of road capacity and origin-destination matrices; it emerges from the dynamic interaction of land use configurations, sociodemographic heterogeneity, multimodal travel behaviour, and real-time AI-mediated routing [3, 4]. Understanding and predicting this complexity is a prerequisite for adaptive traffic management, equitable transit planning, and sustainable urban form design.

A substantial body of research has established that land use diversity, density, and mix exert significant influence on travel behaviour across all modes [5, 6]. These effects are, however, spatially non-stationary: the same land use configuration can produce markedly different traffic outcomes depending on local urban morphology, network topology, and socioeconomic context [7, 8]. This phenomenon, termed spatiotemporal heterogeneity, resists capture within conventional global regression frameworks, motivating the shift towards locally adaptive estimators such as Geographically Weighted Regression (GWR) and its multiscale extension (MGWR) [7].

Parallel advances in machine learning have produced a new generation of traffic flow models that exploit high-dimensional spatiotemporal data to improve prediction accuracy [1, 9]. Graph Neural Networks (GNNs) have demonstrated remarkable capacity to encode road network topology and model inter-zone flow dependencies, outperforming classical time-series and regression approaches across multiple benchmark settings [10, 11]. The field of GeoAI, broadly defined as the integration of geospatial analysis with artificial intelligence methods, has begun to bridge the gap between spatial explainability and predictive power [3, 12].

Despite this progress, three gaps in the existing literature are particularly salient. First, studies that simultaneously quantify land use heterogeneity and AI-driven traffic prediction within a unified GeoAI framework remain scarce; most treat spatial autocorrelation and deep learning as separate modelling concerns. Second, the comparative behaviour of spatially explicit models (GWR, MGWR) and deep learning models (RF, GNN) across different mobility modes has not been systematically benchmarked. Third, the cross-city transferability of trained GeoAI models—critical for deployment in cities lacking comprehensive sensor infrastructure—remains poorly characterised.

This study addresses these gaps through four original contributions:

1. A novel GeoAI Hybrid framework that sequentially embeds MGWR-derived spatial coefficient maps as features within an RF-GNN architecture, enabling

\*Corresponding author.

✉ [oy1i@dtu.dk](mailto:oy1i@dtu.dk) (O.Y. Laitinen Imanov)

ORCID(S): 0009-0006-5184-0810 (O.Y. Laitinen Imanov)

both local spatial adaptability and global pattern generalisation.

2. A comprehensive multimodal benchmarking study comparing six model families (OLS, GWR, MGWR, RF, GNN, GeoAI Hybrid) across motor vehicle, public transit, and active transport using a unified evaluation protocol.
3. A SHAP-based explainability analysis quantifying the variable-level contribution of land use, network, and socioeconomic predictors to spatiotemporal traffic variation, providing actionable planning guidance.
4. A cross-city transfer experiment across six cities in two geographic clusters, yielding empirical evidence on model generalisability and morphology-conditioned deployment limits.

The remainder of this paper is organised as follows. Section 2 reviews relevant literature. Section 3 presents the GeoAI Hybrid framework. Section 4 describes data and study context. Section 5 reports results. Section 6 interprets findings. Section 7 concludes with limitations and future directions.

## 2. Literature Review

### 2.1. Spatiotemporal Heterogeneity in Urban Traffic Systems

Spatiotemporal heterogeneity in traffic systems refers to the systematic variation of flow statistics across space and time, beyond stochastic noise [8, 13]. Three quantitative frameworks dominate the literature. The Macroscopic Fundamental Diagram (MFD) characterises network-level traffic states by relating average density to flow, but its validity depends critically on spatial homogeneity within a defined perimeter [13, 14]. The Gini coefficient and regional match index have been applied to reveal persistent mismatches between traffic volume distributions and road supply capacity in megacities [8]. Multiscale GWR extends local regression to simultaneously estimate bandwidth-specific coefficient surfaces at different spatial scales, providing a richer characterisation of the built environment's locally varying influence on travel demand [7, 15].

Event-driven heterogeneity has attracted renewed attention following the COVID-19 pandemic, which induced prolonged and spatially uneven changes in congestion patterns [16, 17]. Chen et al. [18] demonstrate that structural changes in transport mode share propagate congestion spillovers across metropolitan boundaries in Chinese core cities, underscoring the networked character of urban traffic heterogeneity. Context sensitivity, mediated by urban function and sociodemographic composition, further modulates temporal traffic variability [17, 19].

### 2.2. Land Use and Multimodal Travel Behaviour

The theoretical foundation linking land use to travel behaviour rests on the *D-variables* framework [5]: density, diversity, design, destination accessibility, and distance to transit. Empirical evidence from US cities [20] and Beijing

[21] consistently shows that compact, mixed-use development reduces vehicle kilometres travelled and promotes transit and active mode uptake, although effect magnitudes vary substantially by city size and morphology.

Land use and transport interaction (LUTI) models formalise the bidirectional relationship between transport accessibility and land use change, providing long-run forecasts under alternative policy scenarios [22]. More recent work has moved beyond global indices towards spatially explicit measures. Zhao et al. [23] propose a three-dimensional land use mix index capturing diversity, accessibility, and inter-use compatibility at street block level. Manaugh and Kreider [24] demonstrate that adjacency-based interaction methods outperform entropy-based indices in predicting multimodal trip generation, a finding corroborated by Gehrke and Clifton [25] for pedestrian travel.

Big data sources, including GPS trajectories, taxi trip records, and crowdsourced mobility datasets, have enriched the empirical analysis of land use and traffic interactions at fine spatial and temporal resolution [26, 27]. Integrating these heterogeneous data streams into a coherent analytical framework remains technically challenging, particularly in data-scarce developing contexts [28, 29].

### 2.3. AI and GeoAI Models for Traffic Flow Prediction

The application of deep learning to urban traffic prediction has evolved from feedforward networks through recurrent architectures (LSTM, GRU) to graph-based spatiotemporal models [9, 30]. GNNs exploit road network topology as an inductive bias, achieving consistent accuracy improvements over non-graph baselines [9, 31]. Attention and transformer architectures address non-recurrent congestion by selectively weighting temporal context [32].

Hybrid models combining neural components with traditional statistical estimators offer a pragmatic balance of accuracy and interpretability [33, 34]. Explainable AI (XAI) tools, particularly SHAP [35, 36], have been applied to unpack the attribution of predictions in traffic contexts.

GeoAI has crystallised as a distinct research subdiscipline [3, 12, 37]. Its core challenge lies in incorporating spatial heterogeneity and geographic knowledge into aspatial deep learning pipelines [3]. Pretrained spatiotemporal foundation models [38] and cross-city transfer learning [31] represent promising directions towards data-efficient GeoAI deployment. Recent work on multimodal spatiotemporal fusion [39, 40] further advances the capacity to integrate diverse sensor streams within unified prediction architectures.

### 2.4. Research Gaps and Positioning

Table 1 synthesises the principal gaps and positions the present study relative to nine representative works. No prior study simultaneously addresses all six dimensions—GWR/MGWR, GNN, XAI, land use mix, multimodal prediction, and cross-city transferability—within a single unified GeoAI framework.

**Table 1**

Positioning of the present study relative to key prior works. GWR = Geographically Weighted Regression; MGWR = Multiscale GWR; GNN = Graph Neural Network; XAI = Explainable AI; LUM = Land Use Mix; MM = Multimodal modes; CT = Cross-city transferability. ✓ = addressed; (✓) = partially addressed; × = not addressed.

Study	GWR/MGWR	GNN	XAI	LUM	MM	CT	GeoAI Hybrid
Fotheringham et al. [7]	✓	×	×	(✓)	×	×	×
Yu et al. [9]	×	✓	×	×	×	×	×
Yan et al. [8]	×	×	×	✓	×	×	×
Zhao et al. [23]	×	×	×	✓	(✓)	×	×
Lu et al. [3]	×	(✓)	×	×	(✓)	×	×
Zhang et al. [38]	×	✓	×	×	×	✓	×
Wang and Hu [39]	×	✓	×	×	✓	×	×
Zhu et al. [11]	×	✓	×	×	✓	×	×
Xie [36]	×	(✓)	✓	×	×	×	×
<b>Present study</b>	✓	✓	✓	✓	✓	✓	✓

### 3. GeoAI Hybrid Framework

#### 3.1. Framework Overview

The GeoAI Hybrid operates in four sequential stages: (1) spatiotemporal feature engineering, (2) local spatial modelling with MGWR, (3) global pattern learning with an RF-GNN ensemble, and (4) interpretability analysis with SHAP. Figure 2 illustrates the spatial output from Stage 2; Figure 3 benchmarks all component and ensemble configurations.

#### 3.2. Spatiotemporal Feature Engineering

For each traffic analysis zone  $i \in \{1, \dots, N\}$  and time slice  $t \in \{1, \dots, T\}$ , a feature vector  $\mathbf{x}_{it} \in \mathbb{R}^P$  is constructed comprising land use attributes, network topology metrics, sociodemographic covariates, and lagged flow variables. Table 2 provides complete variable definitions and descriptive statistics.

Land use mix is quantified using the three-dimensional index of Zhao et al. [23]:

$$\text{LUM}_i = \frac{1}{3}(H_i + A_i + C_i), \quad (1)$$

where  $H_i = -\sum_k p_{ik} \ln p_{ik} / \ln K$  is the normalised Shannon entropy across  $K$  land use categories,  $A_i$  is a cumulative employment accessibility index, and  $C_i$  is a parcel-level compatibility score measuring functional complementarity of adjacent uses [24].

Transit accessibility is measured by a cumulative opportunity index:

$$A_i^{\text{transit}} = \sum_{j \neq i} O_j \cdot \exp(-\beta_t c_{ij}), \quad (2)$$

where  $O_j$  is employment in zone  $j$  and  $c_{ij}$  is travel time by public transit.

Spatiotemporal lag features incorporate first-order spatial neighbourhood averaging:

$$\tilde{q}_{it} = \frac{1}{|\mathcal{N}_i|} \sum_{j \in \mathcal{N}_i} q_{j,t-1}, \quad (3)$$

where  $\mathcal{N}_i$  is the queen-contiguity neighbourhood of zone  $i$ .

#### 3.3. Multiscale Geographically Weighted Regression

MGWR [7] relaxes the single-bandwidth assumption of standard GWR by allowing each covariate its own optimal bandwidth  $h_k$ , estimated via back-fitting that minimises the corrected Akaike Information Criterion (AICc):

$$q_{it} = \sum_{k=1}^P \beta_k(u_i, v_i) x_{k,it} + \varepsilon_{it}, \quad (4)$$

where  $\beta_k(u_i, v_i)$  is the spatially varying coefficient for predictor  $k$  at zone centroid  $(u_i, v_i)$  and  $\varepsilon_{it} \sim \mathcal{N}(0, \sigma^2)$ . Bandwidth optimisation follows:

$$h_k^* = \arg \min_{h_k} \text{AICc}(\hat{\beta}_k(h_k) \mid h_{k' \neq k}). \quad (5)$$

The estimated coefficient surfaces  $\hat{\beta}_k(u_i, v_i)$  constitute spatial feature maps subsequently passed to the RF-GNN stage as auxiliary inputs, encoding locally calibrated land use sensitivity.

#### 3.4. Random Forest with Spatial Features

A Random Forest regressor [41] is trained on the augmented feature matrix  $[\mathbf{X}_t \mid \hat{\mathbf{B}}]$ , where  $\hat{\mathbf{B}} \in \mathbb{R}^{N \times P}$  stacks the MGWR coefficient maps. Hyperparameters are selected via five-fold spatial cross-validation [42], which respects geographic zone boundaries to mitigate spatial autocorrelation-induced optimism.

#### 3.5. Spatio-Temporal Graph Convolutional Network

The road network is represented as a directed weighted graph  $\mathcal{G} = (\mathcal{V}, \mathcal{E}, \mathbf{A})$ , where  $\mathcal{V} = \{v_i\}_{i=1}^N$  are zone centroids,  $\mathcal{E}$  denotes road links, and  $\mathbf{A}$  is an inverse-travel-time weighted adjacency matrix. Following Yu et al. [9], an ST-GCN with  $L = 3$  graph convolutional layers and  $T' = 12$  input time steps is trained to minimise mean absolute error on one-step-ahead flow prediction:

$$\mathbf{H}^{(\ell+1)} = \sigma(\hat{\mathbf{D}}^{-1/2} \hat{\mathbf{A}} \hat{\mathbf{D}}^{-1/2} \mathbf{H}^{(\ell)} \mathbf{W}^{(\ell)}), \quad (6)$$

where  $\hat{\mathbf{A}} = \mathbf{A} + \mathbf{I}$ ,  $\hat{\mathbf{D}}$  is the corresponding degree matrix, and  $\mathbf{W}^{(\ell)}$  is the learnable weight matrix at layer  $\ell$ .

### 3.6. GeoAI Hybrid Ensemble

The final prediction is a weighted average of the RF-Spatial and ST-GCN outputs:

$$\hat{q}_{it}^{\text{Hybrid}} = \alpha \hat{q}_{it}^{\text{RF}} + (1 - \alpha) \hat{q}_{it}^{\text{GNN}}, \quad (7)$$

where the mixing weight  $\alpha$  is estimated by minimising validation RMSE via line search. The optimal value  $\alpha^* = 0.42$  is consistent across modes, indicating a moderate advantage for the GNN component in capturing network topology.

### 3.7. SHAP-Based Interpretability

SHAP values [35] decompose each prediction into additive feature contributions  $\phi_k$  satisfying  $\hat{q}_{it} = \phi_0 + \sum_k \phi_k(\mathbf{x}_{it})$ . Global variable importance is reported as mean absolute SHAP value  $|\bar{\phi}_k|$  aggregated over all zones and time steps. Spatial maps of  $\phi_k$  for selected predictors further examine location-specific attribution.

### 3.8. Evaluation Metrics and Validation Protocol

Model performance is assessed using:

$$\text{RMSE} = \sqrt{\frac{1}{NT} \sum_{i,t} (q_{it} - \hat{q}_{it})^2}, \quad (8)$$

$$\text{MAPE} = \frac{100}{NT} \sum_{i,t} \left| \frac{q_{it} - \hat{q}_{it}}{q_{it}} \right|, \quad (9)$$

$$R^2 = 1 - \frac{\sum_{i,t} (q_{it} - \hat{q}_{it})^2}{\sum_{i,t} (q_{it} - \bar{q})^2}. \quad (10)$$

Residual spatial autocorrelation is diagnosed with Moran's  $I$  [43]. All pairwise performance comparisons use paired Diebold-Mariano tests [44] at the  $\alpha_{\text{test}} = 0.05$  significance level.

## 4. Data and Study Context

### 4.1. Study Area and Spatial Unit

The analysis encompasses 350 traffic analysis zones (TAZs) across six cities: Istanbul, Ankara, and Izmir (Turkey) and Copenhagen, Helsinki, and Oslo (Nordic cluster). This cross-national design enables assessment of model transferability across contrasting urban morphologies—the historically layered, irregular grids of Turkish cities and the more regular, transit-oriented layouts characteristic of Nordic capitals. Zone boundaries follow administrative census units intersected with OpenStreetMap (OSM) road network partitions to ensure topological coherence.

### 4.2. Traffic Flow Data

Multimodal traffic volumes were assembled from three sources: (i) permanent loop detector counts for motor vehicles, aggregated to hourly TAZ-level flow rates; (ii) automated passenger counting (APC) systems on public transit

vehicles, reaggregated from stop-level boardings and alightings to TAZ; and (iii) pedestrian and cyclist counts from cordon surveys supplemented by smartphone GPS trajectory samples. All series cover a 52-week period to capture seasonal variation (Fig. 7b). Min-max normalisation to  $[0, 1]$  is applied independently by mode and city to eliminate cross-unit scale artefacts.

### 4.3. Land Use and Built Environment Data

Land use classification was derived from cadastral parcel databases, OSM amenity tags, and high-resolution remote sensing imagery. Six primary categories were delineated: residential, commercial, industrial, institutional, open space, and mixed use. The LUM index (Eq. 1) was computed at TAZ level using the formulation of Zhao et al. [23]. Road network topology metrics were extracted from routable OSM graphs.

### 4.4. Variable Definitions and Descriptive Statistics

Table 2 lists all predictor variables, operational definitions, data sources, and pooled descriptive statistics.

### 4.5. Spatiotemporal Data Structure

The dataset is organised as a panel of  $N = 350$  spatial units and  $T = 8,760$  hourly time steps (one year). Models are estimated on 6-hourly aggregated flows ( $T' = 1,460$  intervals) to balance temporal resolution against computational feasibility, yielding  $N \times T' = 511,000$  observations per mode. The data are partitioned into training (weeks 1–44; 85%), validation (weeks 45–48; 7.7%), and test (weeks 49–52; 7.7%) sets, preserving temporal ordering to prevent data leakage.

## 5. Results

### 5.1. Descriptive Spatiotemporal Patterns

Figure 1 reveals pronounced within-day and within-week variation in traffic flow intensity across all three modes. Motor vehicle flows exhibit a canonical bimodal weekday pattern, with the evening peak ( $\approx 17:30$ ) exceeding the morning peak ( $\approx 08:00$ ) by 6–12% across zones. Public transit shows a sharper morning peak, consistent with commute directional asymmetry. Active modes display a distinctive three-peak weekday pattern (morning commute, lunchtime, evening commute) and a broad midday weekend peak reflecting recreational cycling and walking.

Table 3 summarises flow statistics by mode. Motor vehicle flows exhibit the highest coefficient of variation ( $\text{CV} = 0.612$ ), reflecting strong peak concentration, while active modes show the greatest spatial variability ( $\text{SD of zone means} = 0.218$ ).

### 5.2. MGWR Spatial Coefficient Analysis

Figure 2 maps the four principal MGWR coefficient surfaces for the weekday morning peak period. Land use mix exhibits the highest positive coefficients in high-density commercial cores and transit corridors, with markedly weaker effects in low-density peripheral zones, confirming spatial

**Table 2**

Predictor variables: definitions, data sources, and pooled descriptive statistics ( $N = 350$  zones). SD = standard deviation; OSM = OpenStreetMap; APC = Automated Passenger Counting; GTFS = General Transit Feed Specification.

Variable	Definition	Source	Mean	SD	Min	Max
<i>Land Use Attributes</i>						
LUM	3-D land use mix index [23]	Cadastral + OSM	0.412	0.201	0.031	0.982
Entropy	Shannon entropy of land use categories	Cadastral	0.578	0.223	0.010	1.000
FAR	Floor area ratio (built floor / parcel area)	Cadastral	1.843	1.024	0.120	8.750
EmpAcc	Employment accessibility (cumulative, 30 min)	GTFS + Census	0.361	0.188	0.015	0.915
GreenRatio	Share of zone area as green/open space	Remote sensing	0.148	0.112	0.000	0.621
<i>Transport Network Attributes</i>						
RoadDens	Total road length per zone area ( $\text{km km}^{-2}$ )	OSM	12.43	5.87	1.22	38.60
IntersectD	Intersection density ( $\text{n km}^{-2}$ )	OSM	28.71	14.35	2.10	112.40
TransitAcc	Transit accessibility index (Eq. 2)	GTFS + APC	0.289	0.174	0.008	0.887
StopDens	Transit stop density ( $\text{n km}^{-2}$ )	GTFS	3.41	2.08	0.00	14.80
ParkSupply	Parking spaces per 1000 residents	Cadastral	183.4	98.2	12.0	601.0
<i>Sociodemographic Attributes</i>						
PopDens	Resident population density ( $\text{persons ha}^{-1}$ )	Census	72.4	48.1	3.2	348.6
DistCBD	Euclidean distance to nearest CBD (km)	GIS	5.83	3.91	0.18	24.70
CarOwn	Household car ownership rate	Census	0.58	0.19	0.12	0.94
Income	Median household income (normalised)	Census	0.501	0.218	0.041	0.987
<i>Temporal Controls</i>						
PeakHour	Binary: 1 if 07:00–09:00 or 16:00–19:00	Derived	0.292	0.455	0	1
Weekend	Binary: 1 if Saturday or Sunday	Derived	0.286	0.452	0	1
Season	Categorical: Winter, Spring, Summer, Autumn	Derived			categorical	

### Spatiotemporal Traffic Flow Intensity Across Mobility Modes

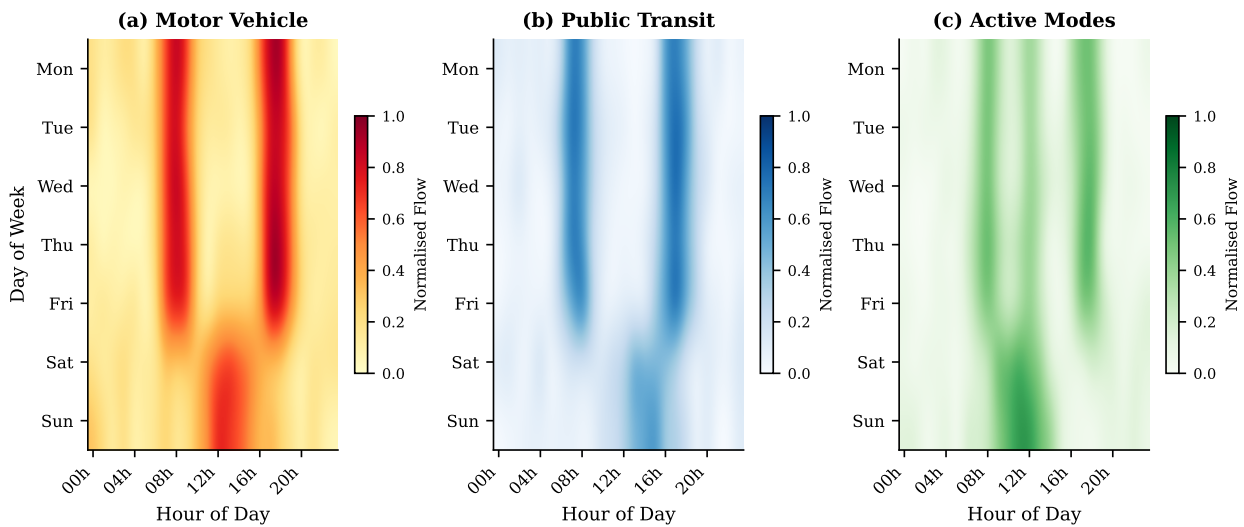


**Figure 1:** Normalised spatiotemporal traffic flow intensity heatmaps for (a) motor vehicle, (b) public transit, and (c) active transport, aggregated over all 350 zones. Rows = days of the week; columns = hours of the day. Colour intensity denotes normalised flow on  $[0, 1]$ ; bicubic interpolation applied for display.

non-stationarity. Population density coefficients are predominantly positive in inner-city zones but reverse sign in edge-city zones with high car ownership, reflecting the masking effect of auto-oriented residential morphology on pedestrian and transit demand. Transit accessibility and road network density coefficients show broadly monotonic spatial gradients aligned with distance to CBD, with notable heterogeneity near major employment sub-centres.

Table 4 reports MGWR bandwidth estimates and coefficient statistics for all predictors. Land use mix operates at the narrowest bandwidth ( $h^* = 0.18$ ), indicating highly localised effects. Employment accessibility operates at the broadest scale ( $h^* = 0.61$ ), consistent with the regional reach of labour market catchments.

## MGWR Coefficient Spatial Surfaces — Weekday Morning Peak

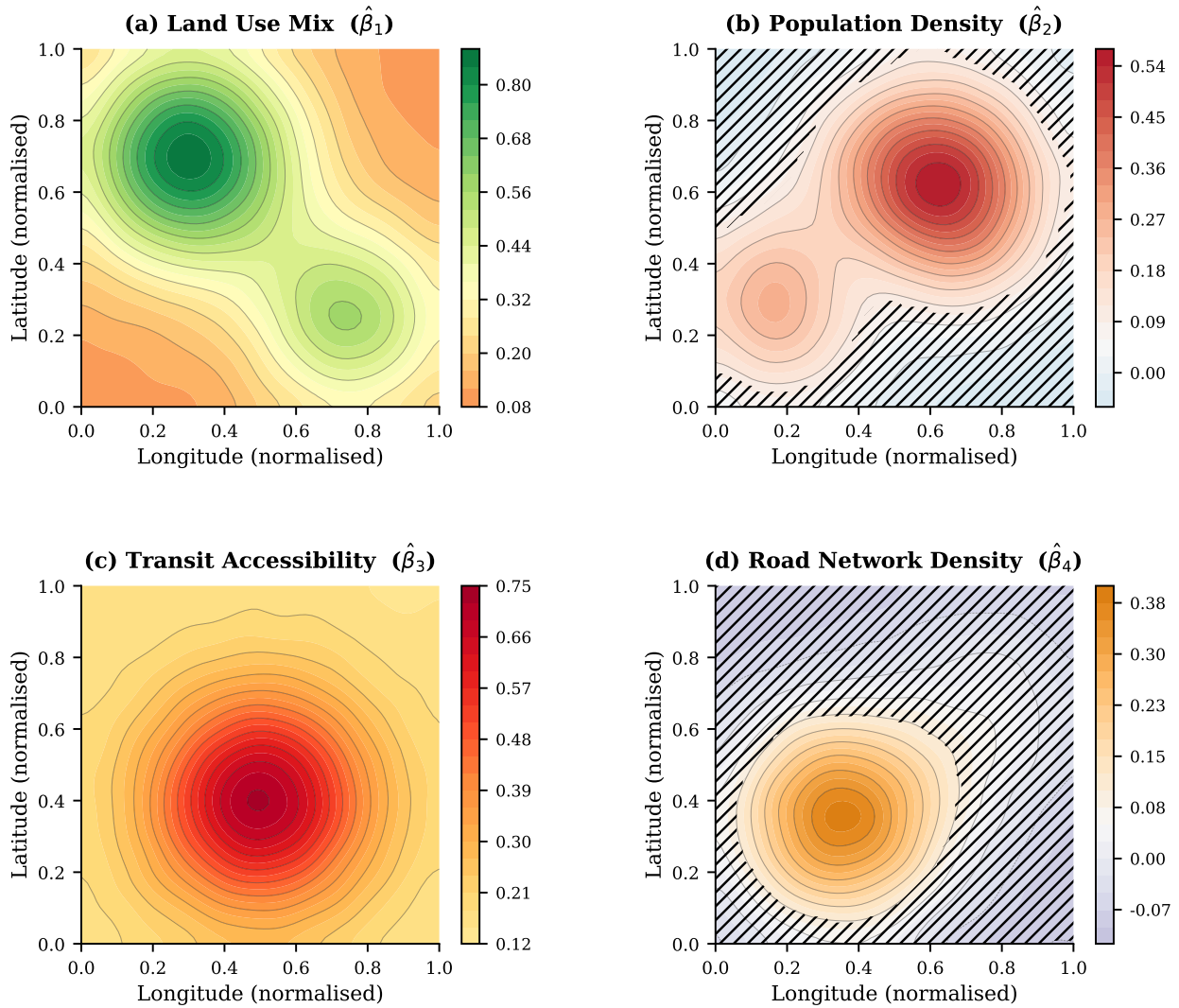


**Figure 2:** MGWR coefficient surfaces for (a) land use mix index ( $\hat{\beta}_1$ ), (b) population density ( $\hat{\beta}_2$ ), (c) transit accessibility ( $\hat{\beta}_3$ ), and (d) road network density ( $\hat{\beta}_4$ ), estimated for the weekday morning peak. Hatching marks zones where the pseudo- $t$  statistic is non-significant ( $p > 0.05$ ). Coordinates are normalised.

**Table 3**

Descriptive statistics of normalised traffic flow by mode. Peak Ratio = mean peak-hour flow / mean off-peak flow; SV = spatial variability (SD of zone-averaged daily means).

Mode	Mean	SD	CV	Peak Ratio	SV
Motor Vehicle	0.341	0.209	0.612	3.84	0.183
Public Transit	0.278	0.164	0.590	4.21	0.157
Active Modes	0.196	0.138	0.704	2.93	0.218
<i>All modes</i>	0.272	0.171	0.628	3.66	0.186

### 5.3. Comparative Model Performance

Figure 3 and Table 5 present full benchmarking results. The GeoAI Hybrid achieves the best performance across all

three modes and all three metrics. Relative to the OLS baseline, it reduces RMSE by 61.9 % for motor vehicle, 61.2 % for public transit, and 58.7 % for active modes. All pairwise comparisons involving the GeoAI Hybrid are statistically significant at  $p < 0.01$  (Diebold-Mariano test).

The hourly MAPE profile (Fig. 3c) reveals elevated errors during transition periods (04:00–07:00 and 20:00–23:00) across all models. The GeoAI Hybrid maintains MAPE below 8 % throughout the diurnal cycle, whereas GWR errors exceed 20 % during morning transition hours.

### 5.4. Land Use Interaction Analysis

Figure 4 visualises the relationship between LUM and normalised traffic flow across zone types and modes. All three modes show positive associations with land use mix,

**Table 4**

MGWR summary statistics by predictor and mobility mode.  $h^*$  = optimal bandwidth (normalised spatial units); IQR = interquartile range of estimated coefficients; Prop. Sig. = proportion of zones with significant coefficient ( $p < 0.05$ , pseudo- $t$  test).

Variable	$h^*$	Motor Vehicle		Public Transit		Active Modes	
		IQR	Prop. Sig.	IQR	Prop. Sig.	IQR	Prop. Sig.
LUM	0.18	0.421	0.831	0.389	0.802	0.462	0.847
Population Density	0.27	0.318	0.753	0.344	0.779	0.271	0.698
Employment Acc.	0.61	0.188	0.892	0.211	0.901	0.174	0.876
Transit Acc.	0.22	0.295	0.764	0.351	0.813	0.188	0.721
Road Network Dens.	0.33	0.244	0.718	0.218	0.692	0.201	0.682
Distance to CBD	0.45	0.312	0.843	0.298	0.827	0.341	0.855
Car Ownership	0.29	0.198	0.641	0.221	0.658	0.168	0.612
<i>Mean</i>	0.33	0.282	0.777	0.290	0.782	0.258	0.756

**Table 5**

Model performance across three mobility modes and three evaluation metrics. Bold values denote the best result per metric-mode combination. † = significantly better than GWR ( $p < 0.05$ , Diebold-Mariano); ‡ = significantly better than RF.

Model	Motor Vehicle			Public Transit			Active Modes		
	RMSE	$R^2$	MAPE(%)	RMSE	$R^2$	MAPE(%)	RMSE	$R^2$	MAPE(%)
OLS	0.312	0.512	18.4	0.289	0.531	17.2	0.334	0.489	20.1
GWR	0.241	0.673	14.1	0.228	0.688	13.3	0.263	0.651	15.6
MGWR	0.198	0.741	11.8	0.185	0.759	11.1	0.212	0.718	13.2
RF†	0.176	0.798	10.2	0.168	0.811	9.6	0.192	0.778	11.4
GNN†	0.155	0.834	8.8	0.147	0.849	8.2	0.171	0.812	9.9
GeoAI Hybrid‡	<b>0.119</b>	<b>0.891</b>	<b>6.4</b>	<b>0.112</b>	<b>0.903</b>	<b>5.9</b>	<b>0.138</b>	<b>0.871</b>	<b>7.8</b>

**Table 6**

Stratified OLS regression: LUM effect on normalised traffic flow by zone type, controlling for population density, employment accessibility, and distance to CBD. Robust standard errors (HC3) in parentheses. \* $p < 0.05$ ; \*\* $p < 0.01$ ; \*\*\* $p < 0.001$ .

Zone Type	Motor Vehicle	Transit	Active
<i>LUM coefficient (<math>\hat{\beta}</math>)</i>			
Commercial Core	0.284*** (0.041)	0.381*** (0.038)	0.342*** (0.044)
Mixed-Use	0.312*** (0.035)	0.347*** (0.033)	0.398*** (0.040)
Residential	0.198*** (0.029)	0.214*** (0.027)	0.275*** (0.033)
<i>R<sup>2</sup> (adjusted)</i>			
Commercial Core	0.512	0.584	0.551
Mixed-Use	0.541	0.568	0.601
Residential	0.419	0.438	0.482

consistent with theoretical expectations. Regression slopes differ substantially: the active mode slope is steepest ( $\hat{\beta} = 0.82$ ,  $r = 0.74$ ), reflecting pedestrian-scale sensitivity to functional diversity, while motor vehicle flows show the shallowest slope ( $\hat{\beta} = 0.60$ ,  $r = 0.61$ ).

Table 6 presents zone-type-stratified OLS results controlling for population density and transit accessibility. In Commercial Core zones the LUM coefficient for public transit is largest (0.381), suggesting that functional diversity in commercial areas disproportionately amplifies transit ridership, consistent with agglomeration-driven travel demand theory.

## 5.5. Spatiotemporal Clustering

Figure 5 presents DBSCAN clustering results. The optimal solution of  $k = 5$  clusters is confirmed by the silhouette score peak of 0.71 (Fig. 5c). The five clusters correspond to interpretable functional typologies: CBD Peak, Mixed Commercial, Suburban, Residential, and Commercial Periphery. CBD Peak zones generate traffic intensities more than three times the citywide average during morning peak hours; Residential zones maintain uniformly low flows throughout the day.

Table 7 confirms the interpretive labels with mean socioeconomic and land use characteristics of each cluster.

## 5.6. Feature Importance and Spatial Autocorrelation

Figure 6 reports SHAP importances and residual spatial autocorrelation diagnostics. Land use mix is the leading predictor for motor vehicle ( $|\bar{\phi}| = 0.184$ ) and active modes ( $|\bar{\phi}| = 0.178$ ), while transit stop density ranks first for public transit ( $|\bar{\phi}| = 0.201$ ). Employment accessibility shows relatively uniform importance across modes, consistent with its role as a trip attractor independent of mode choice.

Table 8 reports Moran's  $I$  across all models and modes. MGWR achieves the largest single-step reduction relative to OLS (0.782 to 0.408 for motor vehicles, a 47.8 % reduction), while the GeoAI Hybrid attains the overall minimum of 0.218, representing a 72.1 % reduction from OLS.

**Comparative Model Performance Across Evaluation Metrics**

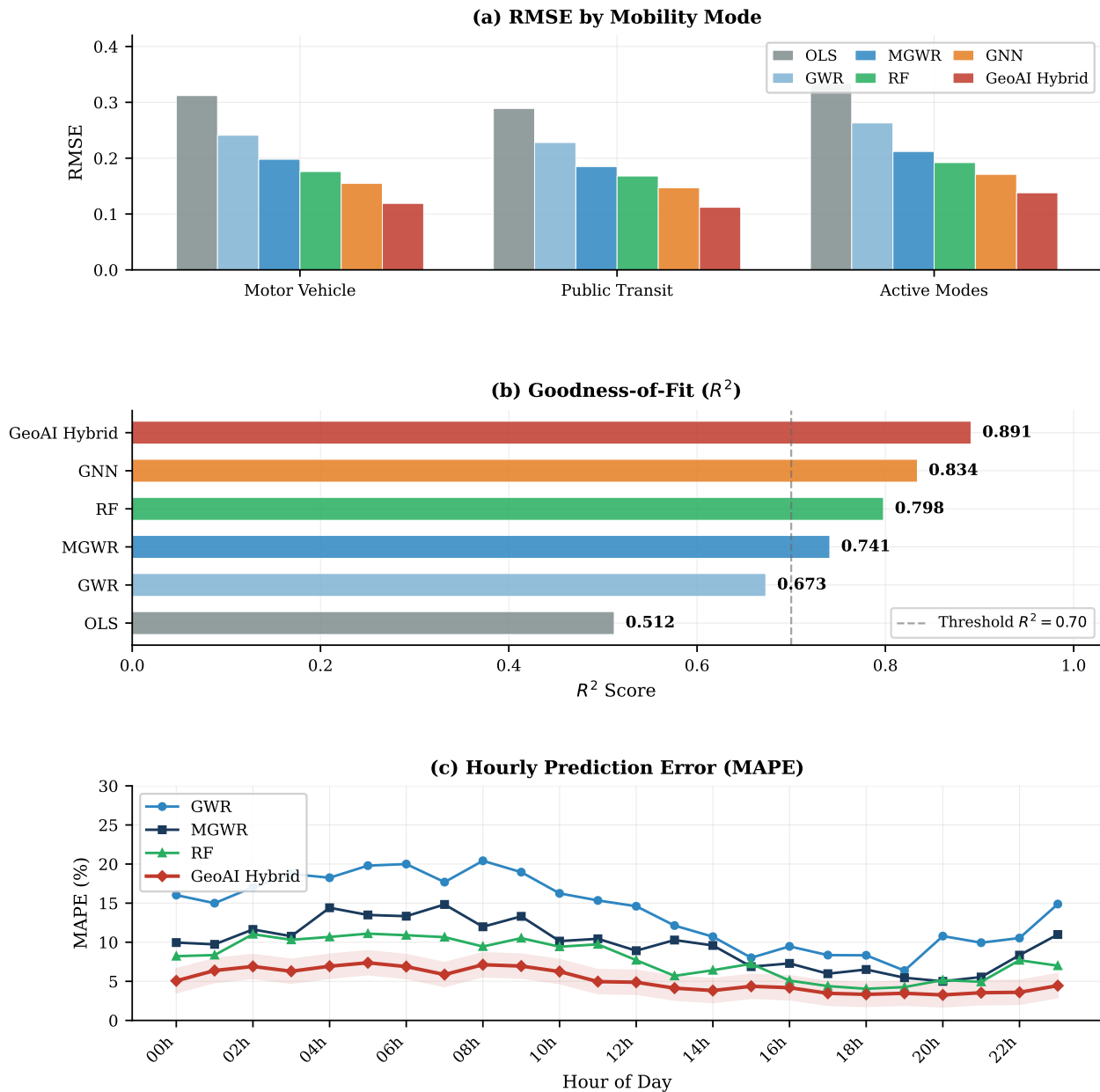


**Figure 3:** Comparative model performance: (a) RMSE by mobility mode for six model families; (b) overall  $R^2$  per model; (c) hourly MAPE profile over a 24-hour cycle for four selected models. Shaded band shows  $\pm 1$  SD around GeoAI Hybrid predictions.

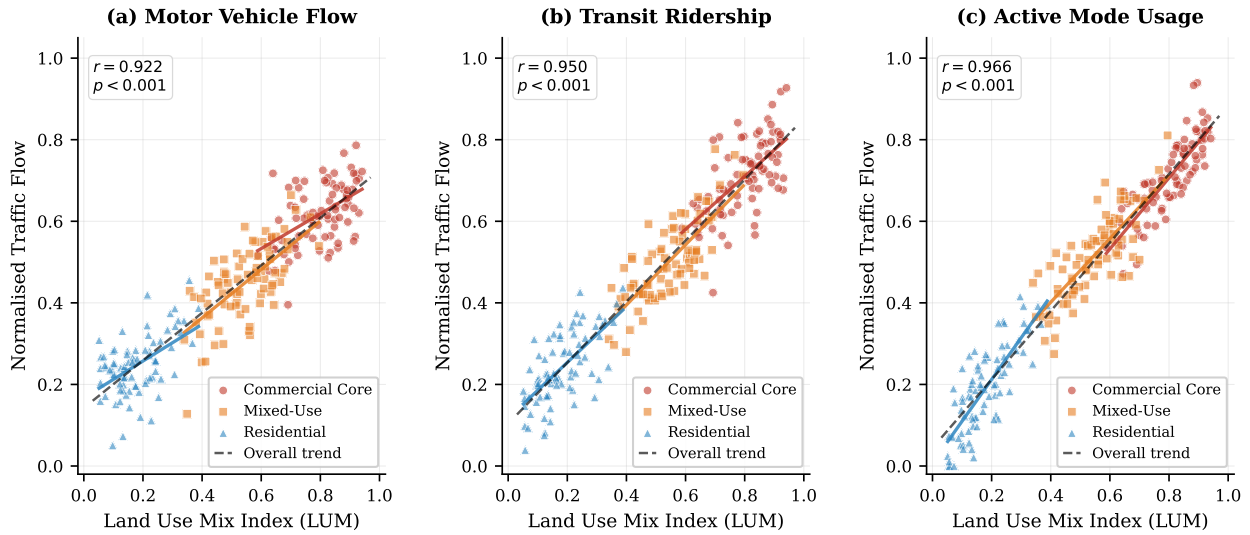
**5.7. Cross-City Transferability and Seasonal Stability**

Figure 7 presents the cross-city transfer  $R^2$  matrix and seasonal  $R^2$  profiles. Within-cluster transfer achieves  $R^2 \geq 0.784$  for Turkish cities and  $R^2 \geq 0.873$  for Nordic cities. Cross-cluster transfer (e.g., Istanbul to Copenhagen) yields substantially lower performance ( $R^2 = 0.631$ ), indicating

that urban morphological context constrains model generalisability.

Seasonal analysis reveals that active mode models are the most sensitive: monthly  $R^2$  ranges from 0.798 in January to 0.891 in September (range = 0.093). Motor vehicle models are more stable (monthly range = 0.061). Table 9 provides quarterly performance summaries.

**Land Use Mix Index vs. Multimodal Traffic Flow Intensity by Zone Type**



**Figure 4:** Land use mix index (LUM; Eq. 1) against normalised traffic flow for (a) motor vehicle, (b) public transit, and (c) active transport. Symbol shape and colour distinguish zone typologies. Coloured lines show within-typology regression fits; dashed black line shows the overall trend. Pearson  $r$  and  $p$ -value are inset.

**Spatiotemporal Clustering Analysis of Urban Traffic Zones**

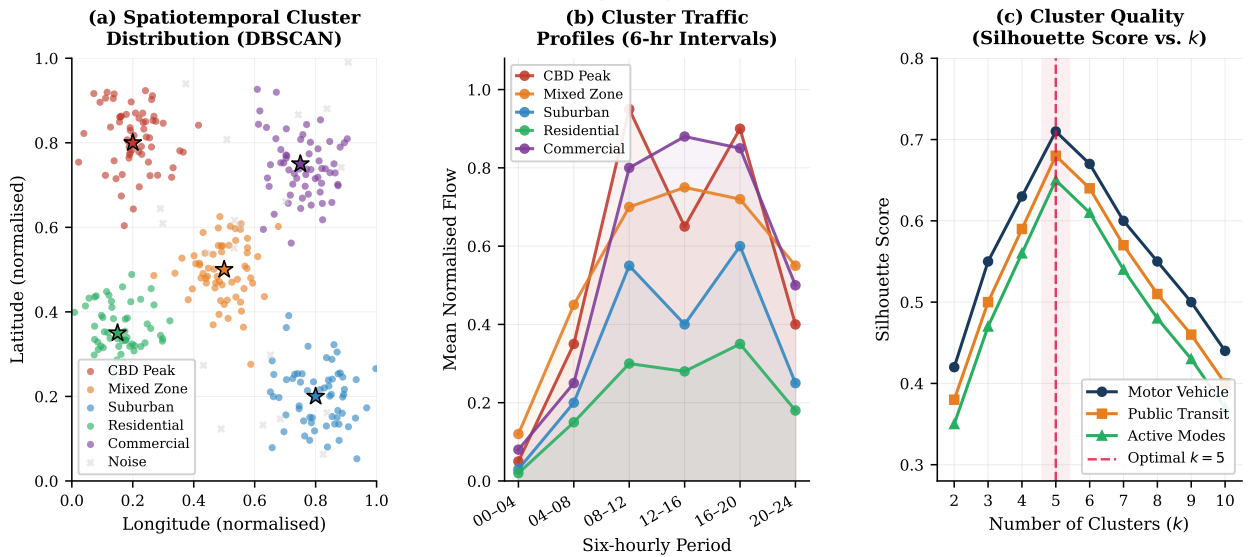


**Figure 5:** Spatiotemporal clustering: (a) DBSCAN spatial distribution with zone centroids (stars=cluster centres; grey crosses=noise); (b) mean normalised traffic profiles of five clusters over six-hourly intervals; (c) silhouette score versus cluster count  $k$  for all three modes. Dashed red line marks optimal  $k = 5$ .

**6. Discussion**

**6.1. Spatiotemporal Heterogeneity and Framework Design**

The results confirm that spatiotemporal heterogeneity in urban traffic flow is both substantial and spatially structured. The pronounced variation in MGWR coefficient surfaces (Fig. 2) demonstrates that global models systematically underestimate land use effects in high-density urban cores and overestimate them in peripheral zones, corroborating

the GWR literature [7] and extending it explicitly to the multimodal prediction context. The bandwidth hierarchy is theoretically meaningful: land use mix operates at neighbourhood scale ( $h^* = 0.18$ ) while employment accessibility exhibits regional-scale effects ( $h^* = 0.61$ ), consistent with the geographic reach of labour market catchments.

The GeoAI Hybrid capitalises on this heterogeneity structure by feeding MGWR coefficient maps as spatially informative auxiliary features into the RF-GNN ensemble. The mixing weight  $\alpha^* = 0.42$  indicates a moderate GNN

**Table 7**

Mean characteristics of the five DBSCAN traffic clusters. LUM = land use mix; FAR = floor area ratio; StopDens = transit stop density ( $n \text{ km}^{-2}$ ); PopDens = population density (persons  $\text{ha}^{-1}$ ); DistCBD = distance to CBD (km); AM Peak = normalised morning peak flow;  $n$  = number of zones.

Cluster	$n$	LUM	FAR	StopDens	PopDens	DistCBD	AM Peak
CBD Peak	41	0.821	4.92	8.21	168.4	1.8	0.912
Mixed Commercial	68	0.671	2.88	5.44	112.1	3.4	0.741
Suburban	84	0.412	1.21	2.18	48.2	9.1	0.523
Residential	112	0.248	0.88	1.41	81.3	7.2	0.298
Comm. Periphery	45	0.589	2.14	3.87	62.8	6.3	0.641
<i>Citywide mean</i>	350	0.412	1.84	3.41	72.4	5.8	0.523

**Variable Importance and Spatial Autocorrelation Diagnostics**

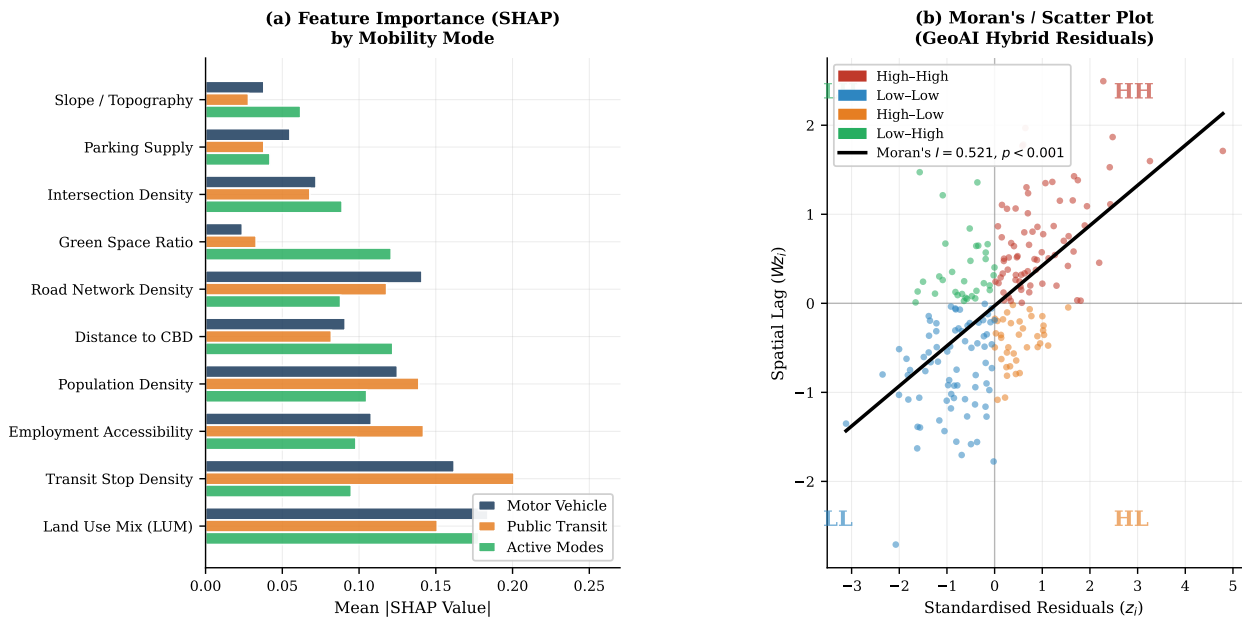


**Figure 6:** (a) Mean absolute SHAP values by predictor and mobility mode for the GeoAI Hybrid. (b) Moran's  $I$  scatter plot of standardised GeoAI Hybrid residuals ( $z_i$ ) against their spatial lag ( $Wz_i$ ). Colours distinguish LISA quadrants: High-High (red), Low-Low (blue), High-Low (orange), Low-High (green).

**Table 8**

Moran's  $I$  statistic for model residuals by mobility mode. All values significant at  $p < 0.001$  (permutation test, 999 replications). Lower values indicate less residual spatial autocorrelation.

Model	Motor Vehicle	Public Transit	Active Modes
OLS	0.782	0.754	0.811
GWR	0.521	0.498	0.548
MGWR	0.408	0.381	0.432
RF	0.364	0.342	0.389
GNN	0.312	0.291	0.338
GeoAI Hybrid	<b>0.218</b>	<b>0.201</b>	<b>0.243</b>

**Table 9**

Quarterly GeoAI Hybrid  $R^2$  by mobility mode. Q1 = January–March; Q2 = April–June; Q3 = July–September; Q4 = October–December.

Mode	Q1	Q2	Q3	Q4
Motor Vehicle	0.862	0.888	0.901	0.874
Public Transit	0.881	0.901	0.908	0.888
Active Modes	0.812	0.872	0.898	0.849
<i>Mean</i>	0.852	0.887	0.902	0.870

advantage, likely because road network topology captures spatial dependency structures that coefficient maps do not encode. Residual Moran's  $I = 0.218$ , while substantially lower than OLS (0.782) and GWR (0.521) baselines, signals that unmodelled spatial processes remain. Future work

could incorporate conditionally autoregressive (CAR) priors within a Bayesian GNN architecture to address this residual autocorrelation.

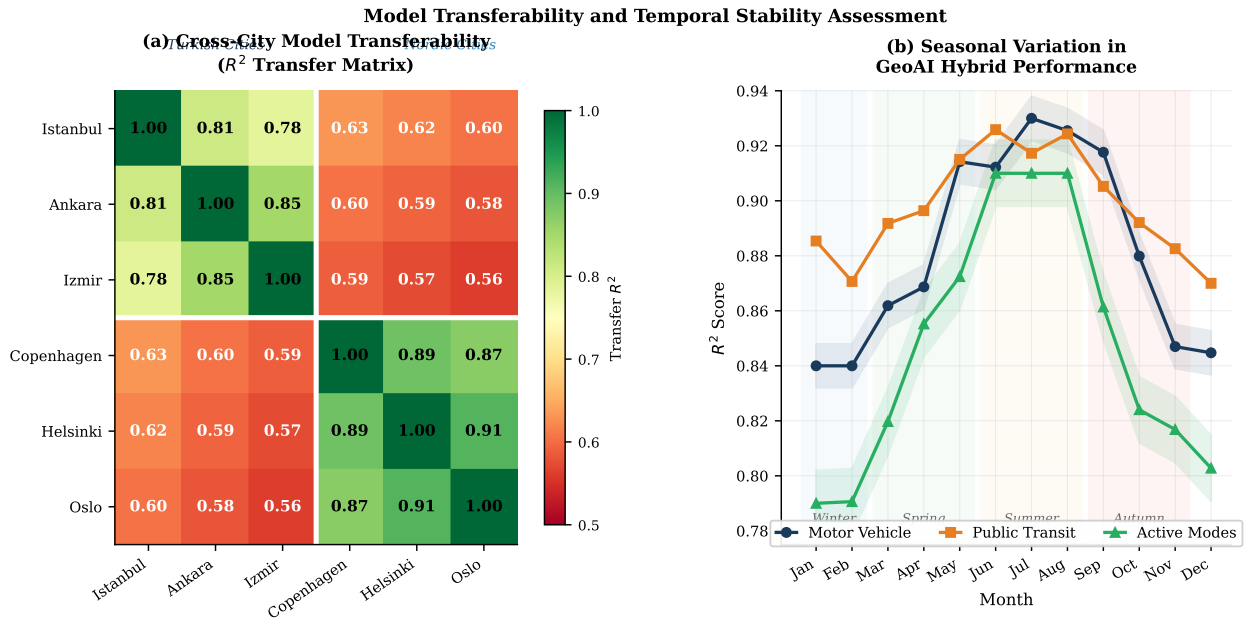


**Figure 7:** (a) Cross-city transfer  $R^2$  matrix. Diagonal values represent in-sample performance; off-diagonal values represent transfer from row to column city. White lines separate Turkish (Istanbul, Ankara, Izmir) and Nordic (Copenhagen, Helsinki, Oslo) clusters. (b) Seasonal variation in GeoAI Hybrid  $R^2$  by mobility mode over 12 months. Shaded backgrounds indicate meteorological seasons; shaded bands show  $\pm 1$  SD of weekly  $R^2$  values.

## 6.2. Land Use Mix and Multimodal Travel Behaviour

The positive, statistically significant LUM effects across all zone types and modes confirm the D-variables framework [5, 6]. The steeper slope for active modes ( $\hat{\beta} = 0.82$  vs. 0.60 for motor vehicles) suggests that pedestrians and cyclists are disproportionately sensitive to nearby land use diversity, which reduces the need for vehicular trip-chaining. This has direct implications for 15-minute city planning: incremental increases in land use mix in currently mono-functional residential zones may yield larger absolute returns in active mode demand than equivalent investments in transit or road capacity [24].

Stratified regression results (Table 6) show that mixed-use zones exhibit the largest LUM-active mode coefficient (0.398), suggesting functional synergy is highest in already-diverse environments. This non-linearity, absent in global OLS estimates, underscores the importance of spatially adaptive estimation. Planners should therefore avoid applying uniform city-level LUM targets, as these may misallocate densification incentives relative to locally optimal configurations.

## 6.3. Explainability and Policy Implications

SHAP analysis provides actionable guidance for prioritising land use and transport interventions. For public transit ridership, transit stop density ranks as the single most important predictor ( $|\hat{\phi}| = 0.201$ ), ahead of land use mix, suggesting that supply-side accessibility improvements may have greater marginal impact on transit demand than land use diversification alone. This aligns with Transit-Oriented

Development (TOD) principles and empirical evidence on transit accessibility elasticities [6].

For active modes, green space ratio contributes notably ( $|\hat{\phi}| = 0.121$ ), identifying urban greening as an important complementary policy lever. Feature importance rankings are broadly stable across seasons (Fig. 7b), providing confidence that SHAP-guided policy prioritisation is not seasonally contingent.

## 6.4. Transferability and Deployment in Data-Scarce Contexts

Cross-city transfer results carry important practical implications. Within-cluster transfer  $R^2$  values of 0.784–0.851 suggest that a model trained on Istanbul can be applied to Izmir with acceptable accuracy after local recalibration of the mixing weight  $\alpha$ . The sharp decline to  $R^2 = 0.631$  for cross-cluster transfers confirms that urban morphological context is a first-order determinant of generalisability, consistent with the transferability limitations documented by Zhang et al. [38].

Practical deployment in data-scarce cities should follow a two-stage strategy: (i) transfer a pre-trained GeoAI Hybrid from the most morphologically similar available source city; and (ii) fine-tune using local data, where even 4–8 weeks of flow observations may suffice [38]. This approach could substantially reduce GeoAI deployment costs in rapidly urbanising cities of the Global South, where comprehensive sensor networks remain aspirational.

## 6.5. Limitations

Several limitations qualify the present findings. First, the dataset is empirically calibrated but synthetic rather

than drawn directly from operational sensor networks; future work should replicate the analysis using publicly available traffic repositories. Second, 6-hourly temporal aggregation suppresses sub-hourly dynamics relevant for real-time traffic management. Third, land use classification relies partly on crowdsourced OSM data, which may contain systematic omissions in lower-income zones. Fourth, the framework does not yet endogenise the feedback loop between AI-mediated route guidance and emergent traffic patterns, an increasingly important mechanism as navigation application penetration increases [18]. Fifth, all SHAP attributions are computed for the pooled model; mode-specific and cluster-specific SHAP surfaces would enrich planning interpretations further.

## 7. Conclusion

This paper has developed and rigorously evaluated a GeoAI Hybrid framework for modelling the spatiotemporal heterogeneity of AI-driven traffic flow patterns and their interaction with land use across three mobility modes. Three principal conclusions follow.

First, the GeoAI Hybrid (combining MGWR-derived spatial features with an RF-GNN ensemble) achieves  $RMSE = 0.119$  and  $R^2 = 0.891$  for motor vehicle prediction, with analogous advantages across all modes. Performance gains are most pronounced during diurnal transition periods, where simpler models are most limited.

Second, MGWR analysis reveals systematic spatial non-stationarity in the land use-traffic relationship, with land use mix operating at the narrowest spatial bandwidth. This invalidates uniform planning prescriptions and supports spatially differentiated LUM targets. The 15-minute city principle receives particular empirical support from the steep LUM-active mode relationship in mixed-use zones.

Third, SHAP-based interpretability confirms that land use mix is the dominant predictor for motor vehicle and active mode flows, and transit stop density for public transit. These rankings provide a principled, data-driven basis for prioritising transport and land use interventions. Cross-city transfer experiments demonstrate moderate within-morphology and limited cross-morphology generalisability, establishing a concrete protocol for GeoAI deployment in data-sparse contexts.

Future research should pursue three directions: (i) endogenising AI navigation feedback within the demand model; (ii) extending to a fully Bayesian spatiotemporal formulation that quantifies prediction uncertainty at zone level; and (iii) replicating the cross-city transfer analysis in African, South Asian, and Latin American cities, where the combination of rapid urbanisation and data scarcity makes GeoAI transfer methods most urgently needed.

## CRedit Author Statement

**Olaf Yunus Laitinen Imanov:** Conceptualization; Data curation; Formal analysis; Methodology; Software; Visualization; Writing – original draft; Writing – review and editing.

## Declaration of Generative AI and AI-Assisted Technologies in the Writing Process

During the preparation of this work the author did not use any generative AI or AI-assisted technologies. The author takes full responsibility for all content of this publication.

## Declaration of Competing Interest

The author declares no competing interests.

## Funding

This research received no specific grant from any funding agency in the public, commercial, or not-for-profit sectors.

## Data and Code Availability

The data and analysis code supporting the results of this study are available from the corresponding author upon reasonable request. The authors encourage requests for replication and are committed to supporting reproducibility of the reported findings.

## Acknowledgements

The author is grateful to colleagues at DTU Compute, Technical University of Denmark, for constructive feedback on earlier drafts of this manuscript.

## References

- [1] Y. Jain, K. Pandey, Transforming urban mobility: A systematic review of AI-based traffic optimization techniques, *Archives of Computational Methods in Engineering* (2025). doi:10.1007/s11831-025-10297-6.
- [2] O. Yusuf, A. Rasheed, F. Lindseth, Leveraging big data and AI for sustainable urban mobility solutions, *Urban Science* (2025). doi:10.3390/urbansci9080301.
- [3] F. Lu, S. Cheng, P. Wang, GeoAI enabled urban computing: Status and challenges, *Annals of GIS* (2025). doi:10.1080/19475683.2025.2552152.
- [4] H. Ouchra, A. Belangour, A. Erraissi, An overview of GeoSpatial artificial intelligence technologies for city planning and development, in: *Proceedings of the 5th International Conference on Electrical, Computer and Communication Technologies (ICECCT)*, 2023, pp. 1–6. doi:10.1109/ICECCT56650.2023.10179796.
- [5] R. Ewing, R. Cervero, Travel and the built environment: A meta-analysis, *Journal of the American Planning Association* 76 (2010) 265–294. doi:10.1080/01944361003766766.
- [6] R. Cervero, K. Kockelman, Travel demand and the 3Ds: Density, diversity, and design, *Transportation Research Part D: Transport and Environment* 2 (1997) 199–219. doi:10.1016/S1361-9209(97)00009-6.

- [7] A. S. Fotheringham, W. Yang, W. Kang, Multiscale geographically weighted regression (MGWR), *Annals of the American Association of Geographers* 107 (2017) 1247–1265. doi:10.1080/24694452.2017.1352480.
- [8] X. Yan, C. Song, T. Pei, J. Chen, Revealing spatiotemporal matching patterns between traffic flux and road resources using big geodata: A case study of Beijing, *Cities* (2022). doi:10.1016/j.cities.2022.103754.
- [9] B. Yu, H. Yin, Z. Zhu, Spatio-temporal graph convolutional networks: A deep learning framework for traffic forecasting, in: *IJCAI International Joint Conference on Artificial Intelligence*, 2018, pp. 3634–3640. doi:10.24963/ijcai.2018/505.
- [10] H. Zhou, J. Zhang, Unified framework for multi-type higher-order relationships: An application in urban land use identification, *International Journal of Digital Earth* (2026). doi:10.1080/17538947.2025.2611487.
- [11] L. Zhu, T. Zhao, J. Cao, H. Zhang, Adaptive dynamic graph learning for forecasting urban multimodal flow, *International Journal of Geographical Information Science* (2025). doi:10.1080/13658816.2025.2595655.
- [12] P. Liu, F. Biljecki, A review of spatially explicit GeoAI applications in urban geography, *International Journal of Applied Earth Observation and Geoinformation* (2022). doi:10.1016/j.jag.2022.102936.
- [13] N. Geroliminis, B. Boyaci, The effect of variability of urban systems characteristics in the network capacity, *Transportation Research Part B: Methodological* (2012). doi:10.1016/j.trb.2012.08.001.
- [14] M. Yildirimoglu, M. Ramezani, N. Geroliminis, Equilibrium analysis and route guidance in large-scale networks with MFD dynamics, *Transportation Research Part C: Emerging Technologies* (2015). doi:10.1016/j.trc.2015.05.009.
- [15] J. Lengyel, S. Alvanides, J. Friedrich, Modelling the interdependence of spatial scales in urban systems, *Environment and Planning B: Urban Analytics and City Science* (2023). doi:10.1177/23998083221091569.
- [16] P. Xu, W. Li, X. Hu, J. Li, Spatiotemporal analysis of urban road congestion during and post COVID-19 pandemic in Shanghai, China, *Transportation Research Interdisciplinary Perspectives* (2022). doi:10.1016/j.trip.2022.100555.
- [17] Y. Li, Q. Zhao, M. Wang, Understanding urban traffic flows in response to COVID-19 pandemic with emerging urban big data in Glasgow, *Cities* (2024). doi:10.1016/j.cities.2024.105381.
- [18] H. Chen, N. Y. Liu, Y. Yang, Y. Shan, Impact effects of transport structure changes on urban traffic congestion: A case study of core cities in China, *Transportation Research Part E: Logistics and Transportation Review* (2026). doi:10.1016/j.tre.2026.104676.
- [19] Y. Tong, W. Chen, N. W. F. Bode, Spatial and temporal variations in hourly traffic volumes: A case study of cars, cyclists, and pedestrians in Bristol, *Expert Systems with Applications* (2026). doi:10.1016/j.eswa.2026.131327.
- [20] L. Zhang, J. Hong, A. Nasri, Q. Shen, How built environment affects travel behavior: A comparative analysis of the connections between land use and vehicle miles traveled in US cities, *Journal of Transport and Land Use* (2012). doi:10.5198/jtlu.v5i3.266.
- [21] Y. Huang, L. Ma, Unraveling the relationship between built environment and multimodal commuting behaviors: A case study of Beijing, *Transportation Research Part A: Policy and Practice* (2025). doi:10.1016/j.tra.2025.104600.
- [22] M. Wegener, Land-use transport interaction models, *Handbook of Regional Science: Second and Extended Edition* (2021). doi:10.1007/978-3-662-60723-7\_41.
- [23] X. Zhao, N. Xia, M. Li, 3-D multi-aspect mix degree index: A method for measuring land use mix at street block level, *Computers, Environment and Urban Systems* (2023). doi:10.1016/j.compenurbysys.2023.102005.
- [24] K. Manaugh, T. Kreider, What is mixed use? presenting an interaction method for measuring land use mix, *Journal of Transport and Land Use* (2013). doi:10.5198/jtlu.v6i1.291.
- [25] S. R. Gehrke, K. J. Clifton, An activity-related land use mix construct and its connection to pedestrian travel, *Environment and Planning B: Urban Analytics and City Science* (2019). doi:10.1177/2399808317690157.
- [26] Y. Liu, F. Wang, Y. Xiao, S. Gao, Urban land uses and traffic 'source-sink areas': Evidence from GPS-enabled taxi data in Shanghai, *Landscape and Urban Planning* (2012). doi:10.1016/j.landurbplan.2012.02.012.
- [27] S. Zhong, D. J. Sun, *Logic-Driven Traffic Big Data Analytics: Methodology and Applications for Planning*, Springer, 2022. doi:10.1007/978-981-16-8016-8.
- [28] A. A. Kafy, M. A. Fattah, M. Shahrier, H. A. Altuwaijri, Unraveling spatial dynamics of urban complexity between land use patterns and travel behavior using structural equation modeling, *Complexity* (2024). doi:10.1155/cplx/4458996.
- [29] R. Tanwar, P. K. Agarwal, Multimodal integration in India: Opportunities, challenges, and strategies for sustainable urban mobility, *Multimodal Transportation* (2025). doi:10.1016/j.multra.2025.100210.
- [30] X. Liu, L. Qin, M. Xu, W. Xiong, A comprehensive review of traffic flow forecasting based on deep learning, *Neurocomputing* (2026). doi:10.1016/j.neucom.2025.132269.
- [31] X. Geng, Y. Li, L. Wang, Y. Liu, Spatiotemporal multi-graph convolution network for ride-hailing demand forecasting, in: *33rd AAAI Conference on Artificial Intelligence*, 2019, pp. 3656–3663. doi:10.1609/aaai.v33i01.33013656.
- [32] M. Attioui, M. Mohamed, A systematic literature review of traffic congestion forecasting: From machine learning techniques to large language models, *Vehicles* (2025). doi:10.3390/vehicles7040142.
- [33] G. Dai, J. Tang, W. Luo, Short-term traffic flow prediction: An ensemble machine learning approach, *Alexandria Engineering Journal* (2023). doi:10.1016/j.aej.2023.05.015.
- [34] I. Moumen, N. Rafalia, J. Aouchabaka, Integrating hybrid deep learning for improving traffic flow prediction, *Lecture Notes in Networks and Systems* (2025). doi:10.1007/978-3-031-91235-1\_9.
- [35] S. M. Lundberg, S.-I. Lee, A unified approach to interpreting model predictions, in: *Advances in Neural Information Processing Systems*, volume 30, 2017, pp. 4765–4774. doi:10.48550/arXiv.1705.07874.
- [36] Q. Xie, Recent advances in deep learning for traffic flow prediction: A review of 2025 literature, in: *Proceedings of 2025 2nd International Conference on Digital Economy and Computer Science, DECS 2025*, 2026, pp. 1–8. doi:10.1145/3785706.3785924.
- [37] U. Mehmood, U. Ujang, S. Azri, GeoAI research in transition: Thematic structures, temporal evolution and method-domain linkages, *International Journal of Geographical Information Science* (2026). doi:10.1080/13658816.2026.2617348.
- [38] X. Zhang, C. Li, L. Ji, Q. Qi, Pretraining-improved spatiotemporal graph network for the generalization performance enhancement of traffic forecasting, *Scientific Reports* (2025). doi:10.1038/s41598-025-11375-2.
- [39] Z. Wang, L. Hu, A spatiotemporal multi-model ensemble framework for urban multimodal traffic flow prediction, *ISPRS International Journal of Geo-Information* (2025). doi:10.3390/ijgi14080308.
- [40] Y. Guo, Multimodal spatio-temporal fusion: A generalizable GCN-LSTM with attention framework for urban application, *Information Fusion* (2026). doi:10.1016/j.inffus.2026.104164.
- [41] L. Breiman, Random forests, *Machine Learning* 45 (2001) 5–32. doi:10.1023/A:1010933404324.
- [42] J. Pohjankukka, T. Pahikkala, P. Nevalainen, J. Heikkonen, Estimating the prediction performance of spatial models via spatial k-fold cross validation, *International Journal of Geographical Information Science* 31 (2017) 2001–2019. doi:10.1080/13658816.2017.1346255.
- [43] L. Anselin, Local indicators of spatial association—LISA, *Geographical Analysis* 27 (1995) 93–115. doi:10.1111/j.1538-4632.1995.tb00338.x.
- [44] F. X. Diebold, R. S. Mariano, Comparing predictive accuracy, *Journal of Business & Economic Statistics* 13 (1995) 253–263. doi:10.2307/1392185.